metals

MDPI

Article

Distribution and Characteristics of Residual Stresses in Super Duplex Stainless Steel Pipe Weld

Chang Beck Cho [1], Joo-Ho Lee [2] and Chin-Hyung Lee [2,*]

[1] Korea Institute of Civil Engineering and Building Technology (KICT), Goyang-si 10223, Gyeonggi-do, Republic of Korea; cbcho@kict.re.kr
[2] Department of Civil and Environmental Engineering, Daelim University College, Anyang-si 13916, Gyeonggi-do, Republic of Korea; joo7777@daelim.ac.kr
* Correspondence: ifinder11@gmail.com; Tel.: +82-31-467-4915

Abstract: This paper explores the distribution and features of residual stresses formed by super duplex stainless steel pipe welding. Experimental investigations, which encompass an elevated temperature tensile test and metallographic observation along with a hardness test and residual stress measurement, were first conducted to obtain the mechanical properties at high base metal temperatures and to confirm whether or not the duplex stainless steel undergoes martensitic phase development during the welding process. Finally, experiments were performed to scrutinize the residual stress evolution through the metallurgical phase transformation in the weld region and its vicinity. A sequentially coupled 3D thermal, mechanical and metallurgical finite element (FE) model capable of incorporating the experimental consequences was established next. A 3D FE simulation of the girth welding process was conducted, and the axial and hoop residual stress profiles along the girth were evaluated. The results substantiate that martensitic phase evolution occurs in the process of cooling during the welding of super duplex stainless steel, and they also highlight the significance of taking the metallurgical phase transformation into account in the numerical reproduction of the girth welding process for the accurate expression of weld-induced residual stresses, which is especially important for precisely predicting hoop residual stresses.

Keywords: super duplex stainless steel pipe; girth weld-induced residual stresses; martensitic phase transformation; 3D thermal; mechanical and metallurgical FE simulation; temperature-dependent material properties

Citation: Cho, C.B.; Lee, J.-H.; Lee, C.-H. Distribution and Characteristics of Residual Stresses in Super Duplex Stainless Steel Pipe Weld. *Metals* **2024**, *14*, 136. https://doi.org/10.3390/met14020136

Academic Editor: Marcello Cabibbo

Received: 8 December 2023
Revised: 6 January 2024
Accepted: 11 January 2024
Published: 23 January 2024

1. Introduction

Duplex stainless steel, which exhibits a microstructure with nearly equal phases of ferrite and austenite, inherits the combined excellent material properties of ferritic and austenitic steels, e.g., outstanding mechanical strength against tension and fatigue, superior toughness and satisfactory weldability, as well as superb resistance to corrosion, pitting and stress corrosion cracking [1]. It is quickly replacing conventional carbon steel and austenitic stainless steel, especially in pipelines for the transportation of liquid and gaseous fuels, such as nitrogen and hydrogen, particularly where chloride or sulfide ions are present. In practice, because of its relatively long geometric configuration compared to diameter and wall thickness, girth butt welding is commonly used to fabricate duplex stainless steel pipe welds [2,3].

Welding is an important joining process and is widely employed in the production of diverse engineering and structural applications, the merits of which include simple arrangement, low manufacturing expenses and highly efficient joints [4,5]. In welded components, undesirable weld-induced residual stresses inevitably exist, which are produced by local plastic strains that are formed due to the non-uniform gradient of temperature during the process of welding. The magnitude and distribution of the residual stresses

can be influenced by several factors, such as the geometry and joint design, the welding process parameters and the metallurgical condition of the material welded. The residual stresses in themselves can be harmful to structural soundness, leading to cracking, stress raising and brittle fractures [6]. When coupled with external loading, these stresses can deteriorate the fatigue strength and promote the crack growth rate. The accurate estimation of weld-induced residual stresses, thus, would greatly help to guarantee the integrity and safety of welded structures. Jiang and colleagues [7] assessed the residual stress distribution of duplex stainless steel multi-pass weld joints via the neutron diffraction and electron backscatter diffraction methods and investigated the formation mechanisms of the residual stresses. Moreover, they proposed a wavelength-dependent neutron diffraction method to measure the residual stresses in thick duplex stainless steel welded plate, and their method was successfully verified by the contour method [8]. Li et al. [9] measured the tensile and compressive residual stresses of square- and H-shaped lean duplex stainless steel welded sections through the non-destructive neutron diffraction method. Based on the experimental results, they recommended analytical models through which to estimate the weld-induced residual stresses of the fabricated sections. All of these works, however, employed experimental techniques to measure the residual stresses in duplex stainless steel welds since predicting residual stresses with accuracy is very challenging work, and this difficulty is attributed to the complexity of the welding process, which involves the use of traveling torches and the dependence of the material properties on temperature, etc. Thus, numerical simulation via the finite element (FE) method has become popular for evaluating weld-induced residual stresses. Meanwhile, it is known that the solid-state phase transformation (SSPT) during welding needs to be incorporated into FE simulations. The volumetric change that occurs in martensitic phase development due to the cooling of the austenitic phase could have a significant impact on the evolution of residual stresses.

A significant number of FE simulations have dealt with the girth welding of steel pipes to identify the residual stresses [10–16]. However, only a few studies have been performed that include an FE analysis of the residual stresses in girth-welded duplex stainless steel pipes. Jin et al. [17] assessed the residual stresses in girth-welded duplex stainless steel pipes (2205 grade); however, their simulation was limited to the rotational symmetry model, which can lessen the cost of computation but may render the analysis to be oversimplified [11]. On the other hand, a 3D FE analysis was conducted by Lee and Chang [18] to compare the residual stresses in austenitic and duplex stainless steel pipe welds. They showed the discrepancies in the magnitude and distribution of the girth-weld-induced residual stresses between them. However, none of these works addressed the metallurgical phase transformation and its relation to the evolution of weld-induced residual stresses. Thus, this work intends to scrutinize the characteristics and distribution of residual stresses produced by the girth welding of super duplex stainless steel pipes by considering the SSPT.

2. Experimental Observation

Experimental investigations, which included a high-temperature tensile test to investigate the material properties of a base metal at elevated temperatures, a metallographic observation and hardness test to identify whether or not the heat-affected zone (HAZ) and the weld metal underwent a martensitic phase evolution associated with the SSPT during welding, and the measurement of residual stress distribution in the welded super duplex stainless steel, were firstly conducted. A 3D thermal, mechanical and metallurgical FE model was established next to predict the girth-weld-induced residual stresses incorporating the experimental consequences. Temperature-dependent material properties, work-hardening behavior and the metallurgical phase transformation were all considered in the FE simulation. From the FE analysis results, the residual stresses in girth-welded super duplex stainless steel pipes were scrutinized.

2.1. Tensile Test at Elevated Temperature

The base metal adopted for this study was S32750 super duplex stainless steel, the material composition and properties of which are given in Table 1. The elevated-temperature tensile test was used to obtain the mechanical properties, such as the yield stress, the ultimate strength and the elastic modulus at ambient and high temperatures, which are necessary input data for the FE welding simulation. The test specimen with spirals at both ends was prepared in accordance with the specifications in Korean standards [19] as shown in Figure 1. A universal testing machine furnished with an electrical furnace (MTS, Eden Prairie, MN, USA) was utilized, and the elevated-temperature tensile test was performed from room temperature to 900 °C with 100 °C intervals and a 1 mm/min strain rate. During the heating process, the temperature was managed to be within ±2 °C while allowing expansion of the specimen by controlling zero tensile force. Each specimen was held for about 20 min. at the target temperature before the testing began to ensure uniform temperature across the specimen. Three specimens were used at the testing temperature to gain the average value.

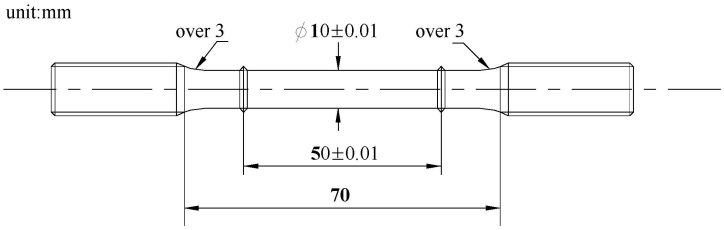

Figure 1. Configuration of the test specimen.

Table 1. Chemical composition and mechanical properties.

Chemical Composition (mass, %)								
C	**Mn**	**P**	**S**	**Si**	**Ni**	**Cr**	**Mo**	**N**
0.019	1.848	0.028	0.0004	0.468	5.065	22.255	2.535	0.1535
Mechanical Properties								
Yield stress (MPa)			Ultimate strength (MPa)			Elongation (%)		
678			839			35		

2.2. Metallographic Observation and Hardness Test

Metallographic observation was conducted to evaluate microstructures in the super duplex stainless steel weld. As indicated before, to accurately simulate weld-induced residual stresses, the SSPT during cooling after heating needs to be taken into account. Furthermore, it is known that conventional high-strength carbon steel with a similar strength grade to the base material experiences martensitic phase transformation during the process of welding [20]. Therefore, it is of critical significance to assess the microstructures of the weld metal and the HAZ, thus verifying whether the metallurgical phase transformation occurs or not.

Two S32750 super duplex stainless steel plates (500 mm × 250 mm × 10 mm) with a single 'V' butt joint configuration between them were prepared to fabricate the weld specimen with six passes via a gas tungsten arc (GTA) welding procedure using Thermanit 22/09 weld filler material. During the welding, the plates were not clamped and preheating was not imposed, and the inter-pass temperature was controlled to remain under 200 °C. The conditions and process parameters of welding are tabulated in Table 2, in which the arc voltage sets were fixed while controlling the heat input by adjusting the welding current and the welding speed. After completion, the microstructures were assessed by using an OLYMPUS PME3 optical microscope (OLYMPUS, Tokyo, Japan). Samples were extracted from the three compositions, i.e., the base metal, the HAZ and the weld

metal at the midpoint of the welding process, which were polished with 1µm diamond paste on a cloth polishing wheel and were etched with Nital's etchant for about 20~30 s. Figure 2a–e represent the microstructures, and it can be observed that the microstructure of the base metal comprises ferrite and austenite with the same volume fraction, and austenite islands in the ferrite matrix were oriented along the rolling direction. In the HAZ microstructure, coarsened ferrite and austenite were found and the arrangement of ferrite and austenite was quite different from the original distribution due to the thermal cycles. On the other hand, the occurrence of distinct forms of austenite, i.e., grain boundary austenite and the intragranular precipitates of austenite, were seen in abundance across the weld metal [21]. In addition to the ferritic and austenitic microstructures, partial martensitic phases were also found in the HAZ and the weld metal from the microstructures with lower magnification. Therefore, it can be inferred that the super duplex stainless steel experiences martensitic phase transformation in the weld metal and the HAZ in the process of cooling during welding.

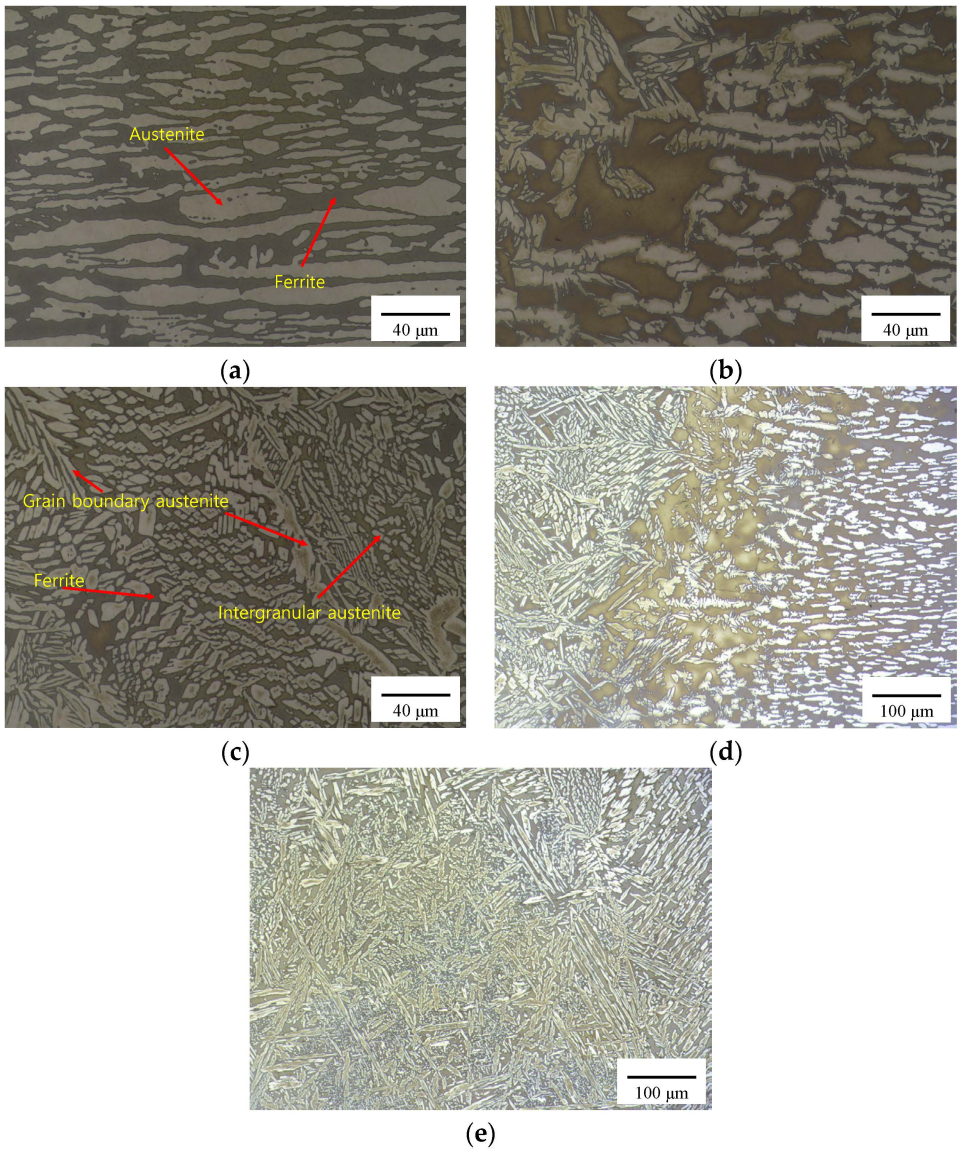

Figure 2. Optical microstructure: (**a**) base metal (×500), (**b**) HAZ (×500), (**c**) weld metal (×500), (**d**) HAZ (×200) and (**e**) weld metal (×200).

Table 2. Welding conditions and process parameters.

PASS	Current (A)	Voltage (V)	Velocity (mm/s)
1	140	12	0.9
2	160	12	1.9
3	170	12	1.7
4	170	12	1.2
5	170	12	1.3
6	160	12	1.0

Hardness measurements were also implemented by utilizing a Vickers hardness (HV10) testing machine (Mitutoyo, Kawasaki, Japan) to evaluate the hardness of the weldpiece. Table 3 lists the averaged hardness values at three points through the thickness across the base metal, the HAZ and the weld metal at the midpoint of the welding process. Referring to the test results, hardening of the HAZ and the weld metal can be identified; this is believed partially to be grain refinement attributed to the recrystallization of the microstructure and partially to be the martensitic phase development observed in the microstructural analysis.

Table 3. Hardness across the weld specimen (HV10).

	Base Metal			HAZ			Weld Metal			HAZ			Base Metal		
Point number	1	2	3	4	5	6	7	8	9	10	11	12	13	14	15
Averaged value	235	236	235	252	252	253	251	254	255	253	255	254	235	235	235

2.3. Residual Stress Measurement

The residual stresses on the surface of the welded duplex stainless steel plate were determined by measuring the released strains with strain gauges employing the sectioning technique, the detailed procedure of which is given in [22]. The measurement points, i.e., the positions of the strain gauges located on the top surface of the welded steel plate, are shown in Figure 3, in which the gauges are intensively attached to the weld region and its vicinity. The measured residual stresses are given in the results section.

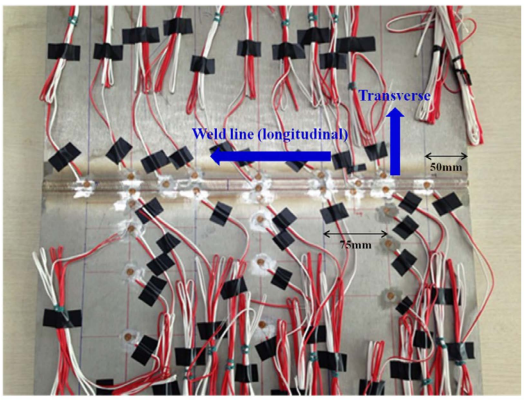

Figure 3. Residual stress measurement location.

3. FE Simulation

3.1. Model Geometry and Material Properties

A 3D thermal simulation using the finite element method (FEM) of the girth-butt-welding process was carried out on a duplex stainless steel pipe with the dimensions of 240 mm (outer diameter) × 240 mm (length) × 6 mm (thickness). The single-pass GTA welding process was employed to join the steel pipes, and the parameters were a voltage

of 22 V, current of 230 A and speed of 1.3 mm/s, analogous to industrial practice [23]. Only one half of the weldpiece was modeled due to the symmetric condition, and the 3D FE model with mesh refinement in the weld region and its vicinity using eight-noded isoparametric solid elements is displayed in Figure 4, where the boundary constraints are indicated by arrows. In the weld and its vicinity in which a high temperature gradient exists, a more refined mesh is required to reproduce an accurate temperature field. Element size becomes incremental with distance from the weld centerline. A mesh convergence study was carried out to assess the dependence of FE mesh size on the accuracy of analysis. As a result, it was determined that the present FE mesh with the smallest element size of 0.9 mm (axial) × 1.5 mm (thickness) × 25.6 mm (circumference) produced sufficiently accurate outcomes while reducing the computational cost. In the FE simulation, the material properties depending on the temperature of the S32750 super duplex stainless steel were taken into consideration. Figure 5 shows varying physical constants (e.g., thermal conductivity, density and specific heat) with temperature [24,25]. As described earlier, the high-temperature mechanical properties were obtained by the experiment. Figure 6 shows the temperature dependency of the mechanical properties, where the yield stress, the tensile strength and Young's modulus are smoothly reduced to the melting point to reproduce the low strength [26]. In this work, autogenous welding is assumed, which implies that the base metal, the HAZ and the weld metal share the same material properties [27].

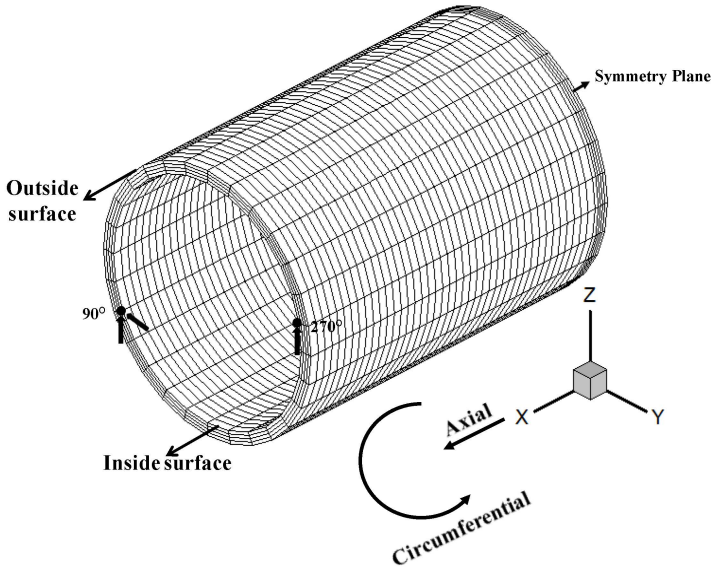

Figure 4. Three-dimensional FE mesh model.

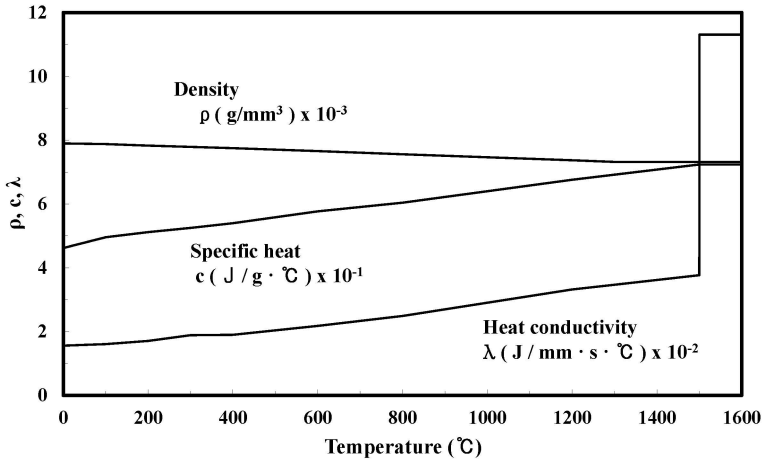

Figure 5. Physical constants at high temperatures.

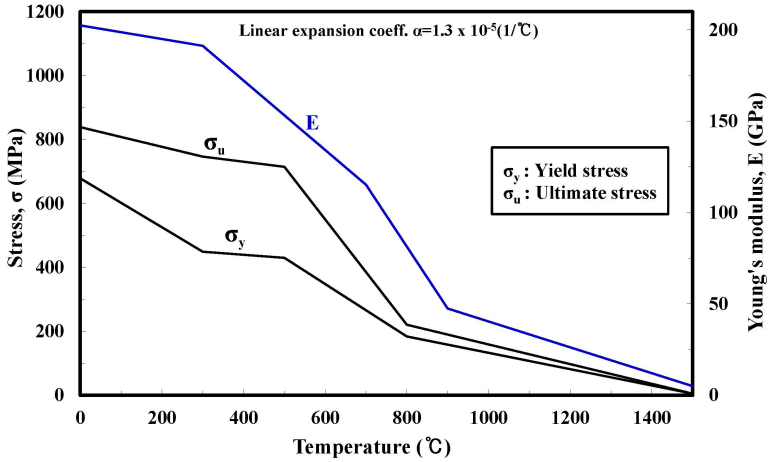

Figure 6. Mechanical properties at elevated temperatures.

During the welding process, since the weld metal and the neighboring base metal are subjected to thermal cycling, the material points in these areas experience repeated plastic deformation. Thus, work hardening occurs in the weld region and its vicinity. Strain hardening has a remarkable effect on the evolution of weld-induced residual stresses and hence was incorporated into the numerical simulation. The duplex stainless steel was regarded to have the same strain-hardening rates at high temperatures as the carbon steels, i.e., linear strain hardening is assumed with the rate of 500 MPa for the temperature range 20~700 °C and 20 MPa for the temperatures above 1000 °C, and a linear transition between the hardening rates at 700 °C and 1000 °C is assumed [28].

3.2. FE Formulation

The numerical simulation of welding requires complex numerical approaches to take the interactions between the heat transfer, the mechanical field and the metallurgical phase transformation into account. The welding process is in essence a coupled thermo-mechanical process in which the temperature and phase evolution significantly affect the structural field with negligible inverted influence. Thus, this study utilizes a sequentially coupled 3D FE formulation based on the in-house FE code [29] to numerically mimic the girth-welding process associated with residual stress evolution. The analysis procedure for weld-induced residual stresses consists of two steps: heat transfer analysis, which determines the heat-flow-induced time-dependent temperature and subsequent phase evolution, followed by mechanical analysis on the basis of the resulting temperature history solutions.

3.2.1. Heat Transfer Analysis

The partial differential governing equation is

$$\frac{\partial}{\partial x}\left(K_x\frac{\partial T}{\partial x}\right)+\frac{\partial}{\partial y}\left(K_y\frac{\partial T}{\partial y}\right)+\frac{\partial}{\partial z}\left(K_z\frac{\partial T}{\partial z}\right)+Q=\rho c\frac{\partial T}{\partial t} \quad (1)$$

where T is the temperature and K, c and ρ stand for the thermal conductivity, the specific heat and the density, respectively. Q signifies the moving heat generation rate per unit volume.

From the viewpoint of the arc welding process, the heat input can be split into two heat sources: the heat from the welding arc and that from the melt droplets, which are modeled by the surface heat source and the volumetric heat source, respectively. Details on the combined heat source model can be found in [12,30]. The heat flux was applied correspondingly to the movement of the welding torch. During the heating and subsequent

cooling, both radiation and convection take place and their coupled impact is reflected by the heat transfer coefficient depending on the temperature h, defined by [10]

$$h = \begin{cases} 0.0668\,T\,(W/m^2\,^\circ C) & 0\,^\circ C < T < 500\,^\circ C \\ 0.231\,T - 82.1\,(W/m^2\,^\circ C) & T > 500\,^\circ C \end{cases} \quad (2)$$

The latent heat of fusion was exploited to model the liquid-to-solid phase transformation of the weld pool, and the augmented thermal conductivity for temperatures above the melting point as shown in Figure 5 was assumed to take the convective stirring effect into account [12]. The latent heat and melting temperature were 500 J/Kg K and 1773 K, respectively [24].

3.2.2. Mechanical (Structural) Analysis

The next step, i.e., the mechanical analysis, utilizes the previous temperature histories for thermal loading for the thermal stress calculation. The two fundamental equations used for the structural analysis are as below.

- Equilibrium equation:

$$\sigma_{ij,j} + \rho b_i = 0 \quad (3)$$

where σ_{ij} indicates the stress tensor and is symmetrical, i.e., $\sigma_{ij} = \sigma_{ji}$, and b_i is the body force.

- Stress–strain constitutive equation:

The incremental form of the relationship can be described by

$$\{d\sigma\} = [\,D_d\,]\{d\varepsilon\} - \{\,c\}dT \quad (4)$$

in which $[\,D_d\,]$ represents the matrix for the stress–strain relationship and is separated into $[\,D_d^e\,]$ and $[\,D_d^p\,]$ for the elastic and the plastic range, respectively, and $\{\,c\}$ comprises parameters which reflect the stress increment owing to the temperature dependence of the material properties. $d\sigma$, $d\varepsilon$ and dT denote the increments of the stress, the strain and the temperature.

The same FE mesh refinement scheme as in the heat transfer analysis was adopted to expedite nodal data mapping between the two analyses, in which the filler activation/deactivation technique [31] was employed to simulate the variation of weld metal deposition with time. The full Newton–Raphson iterative scheme [32] was utilized to solve the nonlinear problem.

3.2.3. Metallurgical Phase Transformation

SSPT is causative of variations in both the volume and the yield stress of steel which undergoes weld-induced thermal cycles and produces transformation-induced plasticity. In super duplex stainless steel weld, the martensitic transformation that occurs during rapid cooling is the phase transformation related to the considerable volume change and the transformation plasticity of the material. During the welding process, as the duplex stainless steel is heated above the A_1 temperature, the ferrite starts to change into austenite, and as the temperature becomes higher than the A_3 temperature, the microstructure is assumed to fully transform into austenite. When the duplex stainless steel is subjected to austenitic phase transformation, it experiences a reduction in volume, as shown schematically in Figure 7. In this study, in accordance with the peak temperature that the material point reaches in the heating process, we determined whether martensitic phase transformation occurs at this point or not, i.e., all the points at which the maximum temperature is higher than the A_3 temperature were regarded to undergo martensitic transformation on cooling to room temperature. Note that the metallurgical phase transformation only takes place in a specific temperature range, i.e., the phase transformation begins to occur at the onset temperature (M_s) and is finished at the end temperature (M_f), which causes volume

expansion as shown in Figure 7 and produces transformation-induced plasticity. The evolution of weld-induced residual stresses caused by the volumetric expansion and the transformation plasticity can be simply simulated by assigning the changed coefficient of thermal expansion to the temperature range of phase transformation [20]. The modified thermal expansion coefficient can be determined through the residual stress measurement, i.e., the extent of residual stress relaxation directly associated with the proportion of martensitic phase transformation can be captured from the experiment and is modeled by adjusting the thermal expansion coefficient in the phase transformation temperature range. Details on the modeling procedure are also specified in [20]. The volumetric reduction during austenitic transformation and the increase in the yield stress that originated in the martensite formation were not considered, since the impacts of the volume and the yield stress change were negligible [28,29].

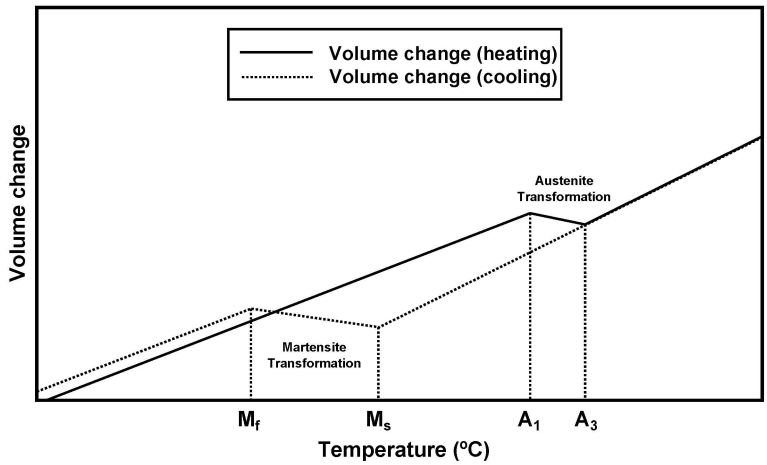

Figure 7. Schematics of the volume changes during austenitic and martensitic phase transformations.

4. Results and Discussion

Results are first reported for the residual stress measurements described in Section 2.3. The symbols shown in Figure 8a represent the measured longitudinal residual stresses (acting parallel to the weld line), which are the most detrimental to the structural integrity, at the mid-length cross-section of the weldpiece perpendicular to the weld line. Note that the distribution and magnitude of the measured residual stresses perpendicular to the weld line along the weld length are very similar to each other, except for the weld start and end regions. The residual stresses are reported at the top layer and are portrayed against the distance from the weld centerline. The lower stresses in the weld metal and the HAZ can be interpreted as being caused by the martensitic phase transformation. For the purposes of verification, a numerical simulation of the welding process with or without taking the SSPT into account was also carried out, and the outcomes were superimposed on the strain gauge measurements. Specific details on the numerical reproduction are given later. It can be seen that the simulated longitudinal stresses that took the metallurgical phase transformation into account agree very well with the experimental measurements; however, the stresses predicted with no consideration of the phase transformation are much higher than the measured residual stresses within and near the weld region. The higher tensile stresses in the weld area and its neighborhood decrease to compressive stresses away from the weld line for self-equilibrium. The distribution of transverse residual stress (acting perpendicular to the weld line, i.e., acting along the plate width) is presented in Figure 8b, in which good agreement between the test results and the simulated prediction is also seen. The transverse stresses are almost totally in tension and gradually converge to zero. Hence, the simulation method employed was considered appropriate for analyzing weld-induced residual stresses and thus can be expanded to predict the residual stresses in girth-welded super duplex stainless steel pipes.

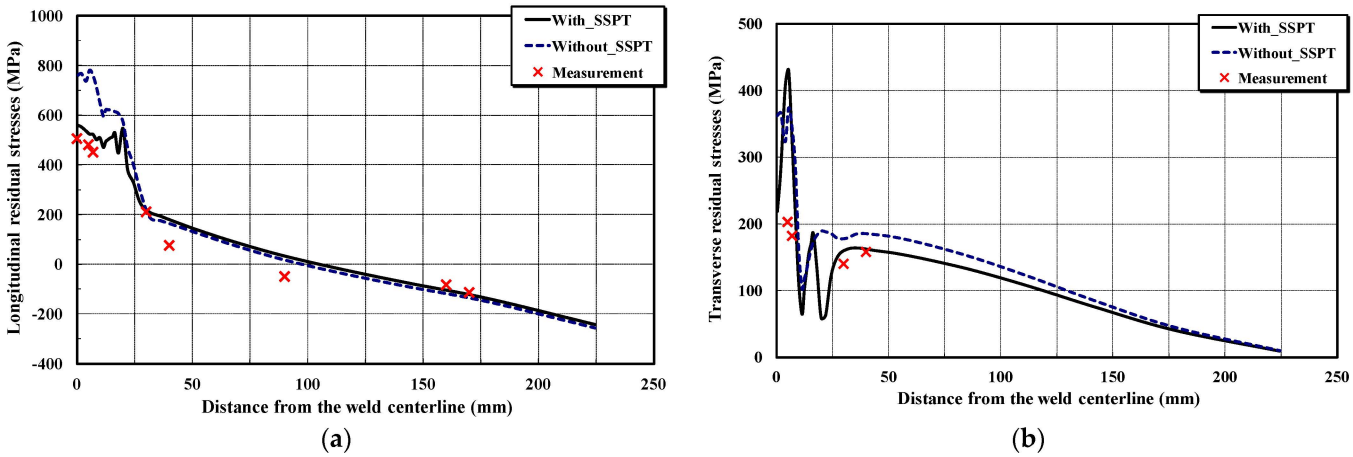

Figure 8. Comparison of the residual stress measurements with the FE analysis results, both with and without considering the SSPT: (**a**) longitudinal residual stresses and (**b**) transverse residual stresses.

Figures 9 and 10 portray the girth-weld-induced axial residual stresses, which act normally in relation to the weld line, along the axial distance on the inside and the outside surfaces (see Figure 4), respectively. The residual stress distributions at different positions along the circumference were reported to explore the 3D effect, i.e., the circumferential variation in the residual stress distribution. The residual stresses simulated without taking the metallurgical phase transformation into account are also reported for comparison. From the simulated results, bending axial stress profiles across the girth-welded pipe thickness can be observed in the weld region and its vicinity, i.e., the axial residual stresses are tensile on the inside surface and compressive on the outside surface along the circumference. The simulated results also reveal that the formation of martensite in the HAZ and the weld metal has little impact on the evolution of axial residual stresses. It is thus inferred that the axial residual stresses are formed primarily by the circumferential shrinkage induced by the cooling process, which leads to local inward deformation at the weld zone, thus resulting in the axial bending moment through the pipe thickness. The compressive stresses are produced on the inside surface and the tensile stresses on the outside surface far from the weld area for self-equilibrating purposes, all of which gradually decrease to zero. It also needs to be recognized that despite the similarity of the residual stress profiles along the circumference on the respective surfaces, the stress values are different from each other. This signifies that the axial stress distribution is sensitive to the circumferential location. This is because the internal constraint varies spatially, which can be attributed to the movement of the welding torch along the girth. In addition, the end effect at the welding start/stop position makes the circumferential variation of the stress profile heavy.

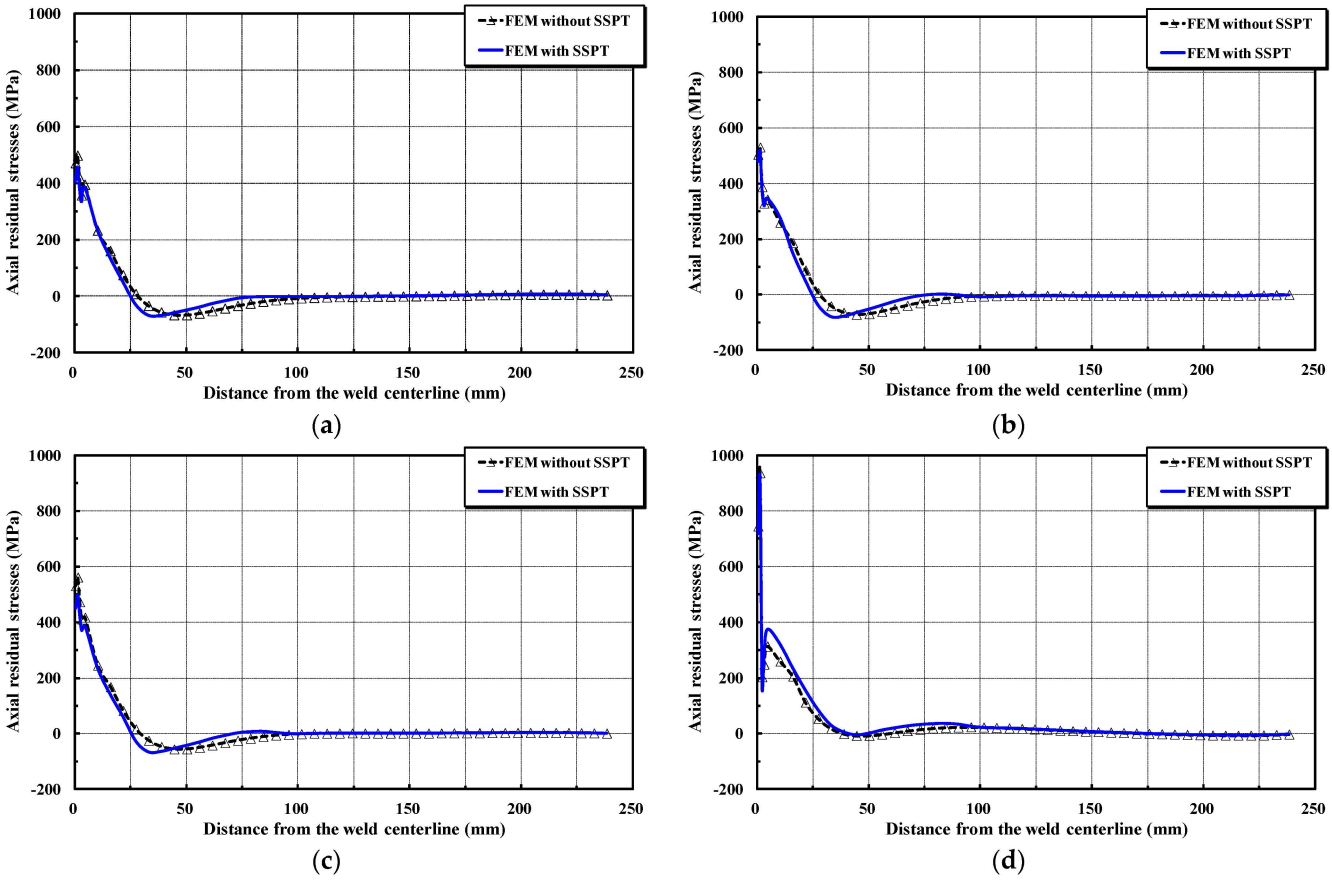

Figure 9. Axial residual stresses on the inside surface at locations with different circumferential angles from the welding start/stop position: (**a**) 90°, (**b**) 180°, (**c**) 270° and (**d**) 360°.

The curves shown in Figures 11 and 12 are the profiles of hoop residual stresses acting parallel to the weld line on the inside and the outside surface, respectively, obtained with and without allowing for the metallurgical phase transformation effect. The results show that the axial residual stresses affect the magnitude and distribution of the hoop residual stresses. This is the reason why the hoop residual stresses in and around the weld region on the outside surface subjected to axial compression are less tensile than those on the inside surface. Analogous to the preceding axial residual stresses, the spatial variation along the girth is present due to the moving arc. In addition, a considerable discrepancy between the hoop stresses that remain in and around the weld zone, which were predicted with and without considering the effect of SSPT, respectively, exists. The lower stresses are attributed to the volumetric expansion of the material points which experience the austenite-to-martensite phase transformation. It also needs to be recognized that the degree of stress relief varies along the circumference. Meanwhile, the hoop stresses in the base metal located just beside the HAZ, where the thermal history does not reach the transformation temperature and thus the metallurgical phase transformation does not occur, rise significantly since there is no volumetric change to relieve the high stresses. The tensile stresses decrease drastically to compressive stresses far from the weld centerline, followed by convergence to zero. A rapid alteration in the hoop residual stresses is also seen in the overlapping region. These results substantiate that both the axial and the hoop residual stress profiles along the girth are not axisymmetric at all, and they also highlight the significance of taking the metallurgical phase transformation into account in numerical simulations of the welding process for an accurate description of the residual stresses in girth-welded duplex stainless steel pipes.

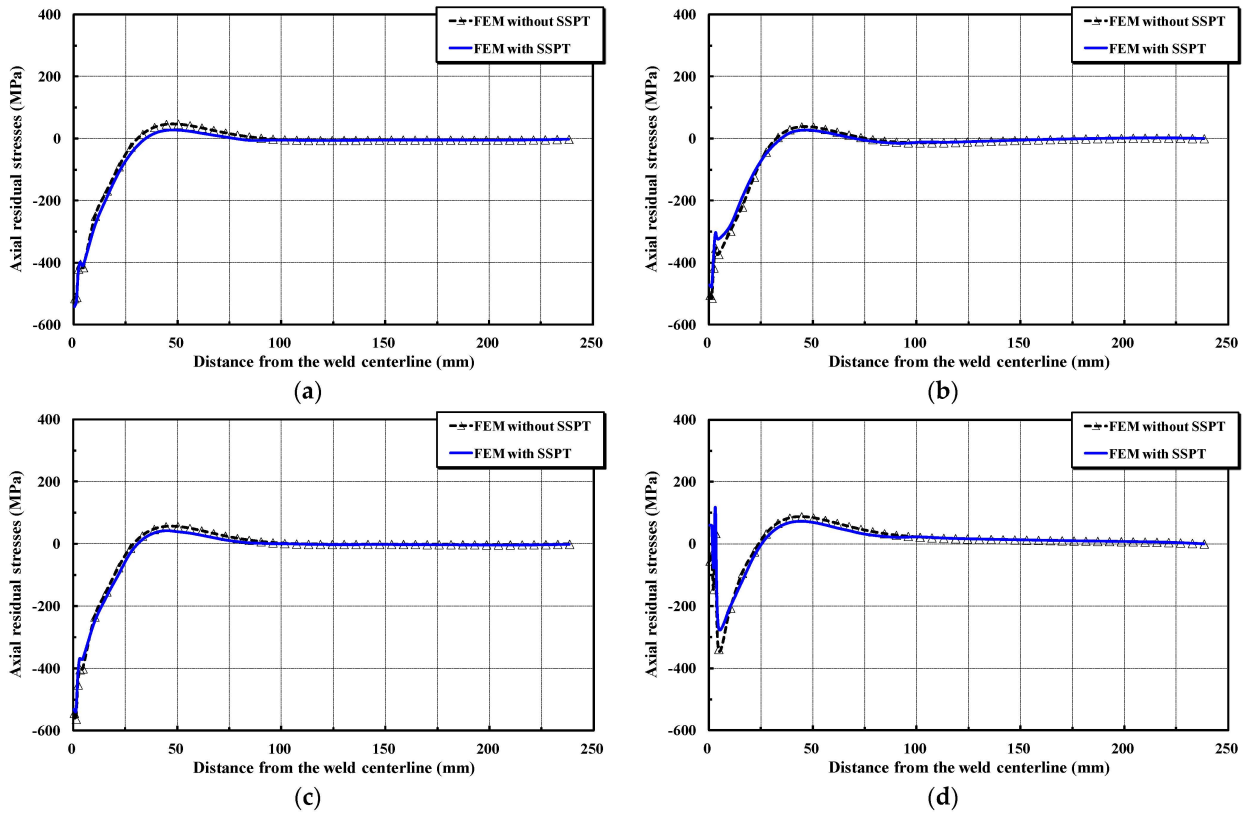

Figure 10. Axial residual stresses on the outside surface at locations with different circumferential angles from the welding start/stop position: (**a**) 90°, (**b**) 180°, (**c**) 270° and (**d**) 360°.

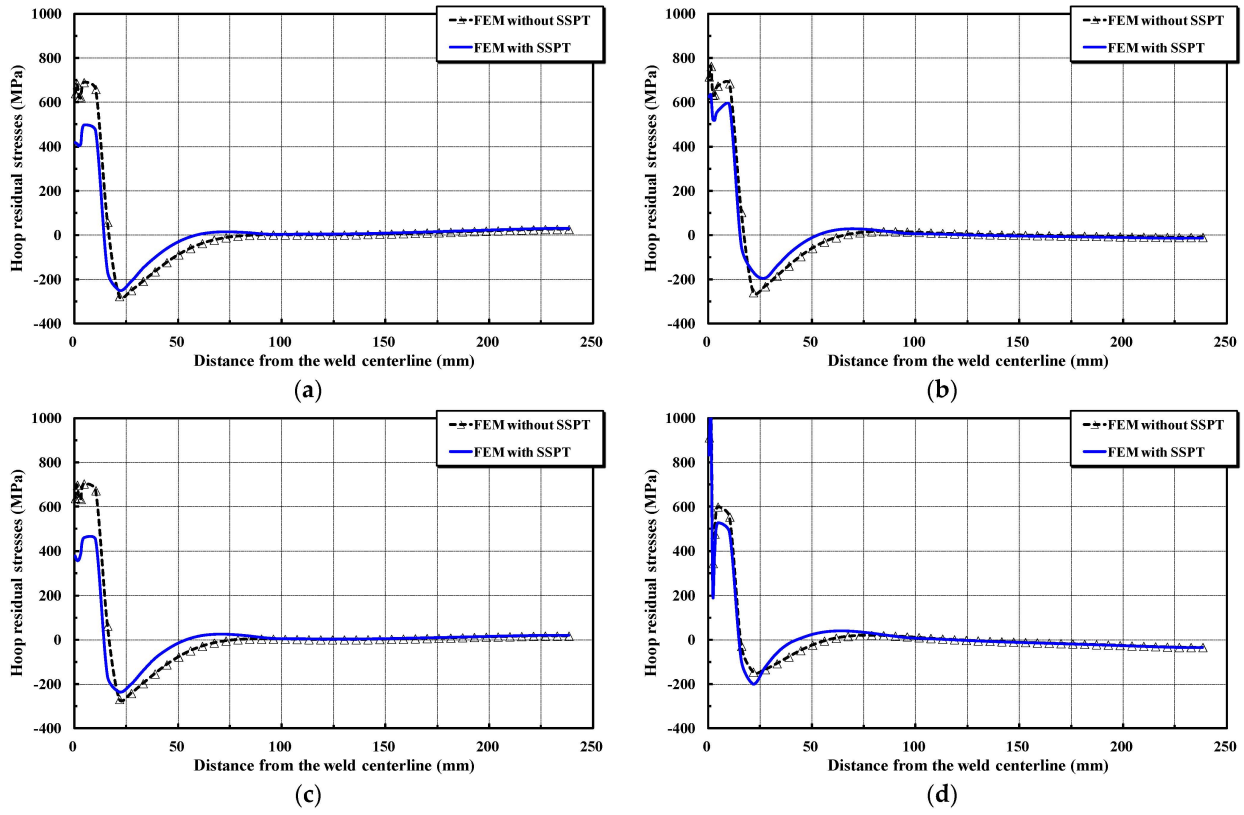

Figure 11. Hoop residual stresses on the inside surface at locations with different circumferential angles from the welding start/stop position: (**a**) 90°, (**b**) 180°, (**c**) 270° and (**d**) 360°.

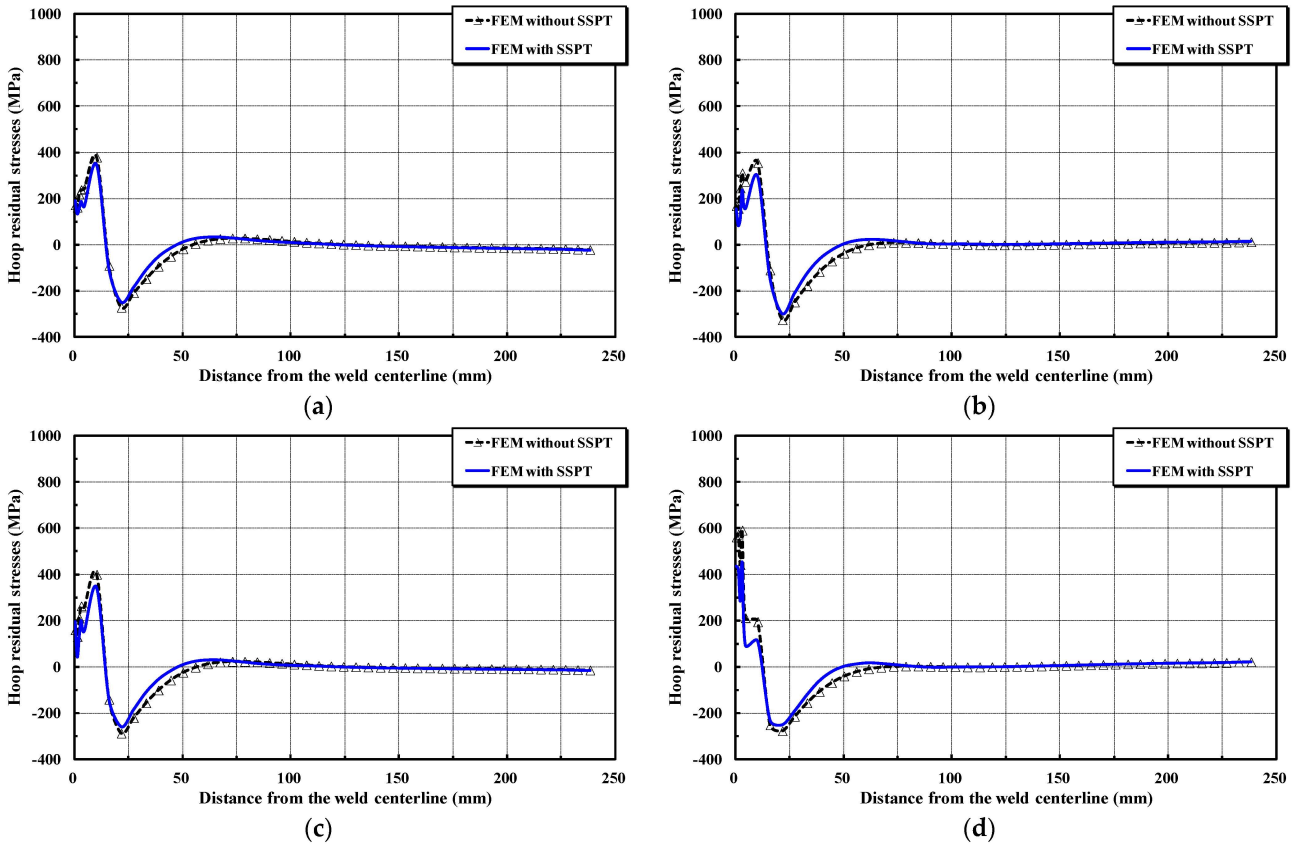

Figure 12. Hoop residual stresses on the outside surface at locations with different circumferential angles from the welding start/stop position: (**a**) 90°, (**b**) 180°, (**c**) 270° and (**d**) 360°.

5. Conclusions

This work, by using an FE simulation technique, reproduces the girth welding of a super duplex stainless steel pipe to elucidate the distribution and features of weld-induced residual stresses. Our experimental investigations included an elevated temperature tensile test to determine the high-temperature mechanical properties, which are a prerequisite to the FE welding simulation, and a metallographic observation along with a hardness test and residual stress measurement to check whether or not the duplex stainless steel experienced martensitic phase transformation during the welding process and to assess the extent of the residual stress relaxation. A sequentially coupled 3D thermal, mechanical and metallurgical FE model able to take the experimental consequences into account was next presented, and its validity was confirmed. The metallurgical phase transformation was incorporated into the FE model through the modified thermal expansion coefficient associated with the volume change. A 3D FE simulation of the girth-welding process was performed, and the axial and the hoop residual stress distributions along the circumference were scrutinized, focusing on the impact of the phase transformation on the axial and hoop residual stress evolution. Based on the achieved outcomes, the following key conclusions can be made:

(a) Super duplex stainless steel undergoes martensitic phase evolution in the HAZ and the weld metal in the process of cooling during welding.

(b) The martensitic phase transformation has little impact on the evolution of axial residual stresses, i.e., the axial residual stresses are mainly formed by circumferential shrinkage during the cooling process. On the other hand, a considerable release of hoop residual stresses in the weld region and its vicinity takes place owing to the volume change in the process of phase transformation. Thus, the metallurgical phase transformation cannot be disregarded in numerical simulations of the girth-welding process to provide an accurate expression of the weld-induced residual stresses.

(c) A 3D FE model should be utilized to accurately simulate the distribution of residual stresses and their characteristics along the circumference in girth-welded super duplex stainless steel pipes, since the residual stresses are by no means axisymmetric, and are caused by both the spatial deposition of the weld filler and the welding start/end effect.
(d) Knowledge of the distribution and characteristics of the residual stresses found in this work can assist the production of an efficient and economic design of welded super duplex stainless steel structures.

Author Contributions: Conceptualization, C.B.C. and C.-H.L.; Methodology, J.-H.L. and C.-H.L.; Software, C.B.C. and J.-H.L.; Validation, C.B.C. and J.-H.L.; Formal analysis, C.B.C. and C.-H.L.; Investigation, C.B.C., J.-H.L. and C.-H.L.; Data curation, C.B.C. and J.-H.L.; Writing—original draft, C.-H.L.; Writing—review and editing, C.B.C., J.-H.L. and C.-H.L.; Visualization, C.B.C. and J.-H.L. All authors have read and agreed to the published version of the manuscript.

Funding: This research was supported by the Korea Agency for Infrastructure Technology Advancement (KAIA) grant funded by the Ministry of Land, Infrastructure and Transport (Grant No. RS-2021-KA163162).

Data Availability Statement: The data presented in this study are available on request from the corresponding author.

Conflicts of Interest: The authors declare no conflicts of interest.

References

1. Iris, A.-A. Duplex stainless steels: Brief history and some recent alloys. *Recent Pat. Mech. Eng.* **2008**, *1*, 51–57.
2. Li, L.; Du, Z.; Sheng, X.; Zhao, M.; Song, L.; Han, B.; Li, X. Comparative analysis of GTAW+SMAW and GTAW welded joints of duplex stainless steel 2205 pipe. *Int. J. Press. Vessel. Pip.* **2022**, *199*, 104748. [CrossRef]
3. Sharma, L.; Sharma, K. Dissimilar welding of super duplex stainless steel (SDSS) and pipeline steel—A brief overview. *Mater. Today Proc.* 2022, *in press*. [CrossRef]
4. Rezanov, V.A.; Martyushev, N.V.; Kukartsev, V.V.; Tynchenko, V.S.; Kukartsev, V.A.; Grinek, A.V.; Skeeba, V.Y.; Lyosin, A.V.; Karlina, A.I. Study of melting methods by electric resistance welding of Rails. *Metals* **2022**, *12*, 2135. [CrossRef]
5. Gonçalves e Silva, R.H.; Barancelli Schwedersky, M.; Fernandes da Rosa, Á. Evaluation of toptig technology applied to robotic orbital welding of 304L pipes. *Int. J. Press. Vessel. Pip.* **2020**, *188*, 104229. [CrossRef]
6. Withers, P.J. Residual stress and its role in failure. *Rep. Prog. Phys.* **2007**, *70*, 2211–2264. [CrossRef]
7. Wan, Y.; Jiang, W.; Song, M.; Huang, Y.; Li, J.; Sun, G.; Shi, Y.; Zhai, X.; Zhao, X.; Ren, L. Distribution and formation mechanism of residual stress in duplex stainless steel weld joint by neutron diffraction and electron backscatter diffraction. *Mater. Des.* **2019**, *181*, 108086. [CrossRef]
8. Jiang, W.; Wan, Y.; Tu, S.-T.; Wang, H.; Huang, Y.; Xie, X.; Li, J.; Sun, G.; Woo, W. Determination of the through-thickness residual stress in thick duplex stainless steel welded plate by wavelength-dependent neutron diffraction method. *Int. J. Press. Vessel. Pip.* **2020**, *196*, 104603. [CrossRef]
9. Li, D.; Paradowska, A.; Uy, B.; Wang, J.; Proust, G.; Azad, S.K.; Huang, Y. Residual stress measurements of lean duplex stainless steel welded sections. *J. Constr. Steel Res.* **2021**, *186*, 106883. [CrossRef]
10. Brickstad, B.; Josefson, B.L. A parametric study of residual stresses in multi-pass butt-welded stainless steel pipes. *Int. J. Press. Vessel. Pip.* **1998**, *75*, 11–25. [CrossRef]
11. Duranton, P.; Devaux, J.; Robin, V.; Gilles, P.; Bergheau, J.M. 3D modeling of multipass welding of a 316L stainless steel pipe. *J. Mater. Process. Technol.* **2004**, *153–154*, 457–463. [CrossRef]
12. Deng, D.; Murakawa, H. Numerical simulation of temperature field and residual stress in multi-pass welds in stainless steel pipe and comparison with experimental measurements. *Comput. Mater. Sci.* **2006**, *37*, 269–277. [CrossRef]
13. Yaghi, A.; Hyde, T.H.; Becker, A.A.; Sun, W.; Williams, J.A. Residual stress simulation in thin and thick–walled stainless steel pipe welds including pipe diameter effects. *Int. J. Press. Vessel. Pip.* **2006**, *83*, 864–874. [CrossRef]
14. Deng, D.; Murakawa, H.; Liang, W. Numerical and experimental investigations on welding residual stress in multi-pass butt-welded austenitic stainless steel pipe. *Comput. Mater. Sci.* **2008**, *42*, 234–244. [CrossRef]
15. Sattari-Far, I.; Farahani, M.R. Effect of the weld groove shape and pass number on residual stresses in butt-welded pipes. *Int. J. Press. Vessel. Pip.* **2009**, *86*, 723–731. [CrossRef]
16. Deng, D.; Kiyoshima, S. FEM prediction of welding residual stresses in a SUS304 girth-welded pipe with emphasis on stress distribution near weld start/end location. *Comput. Mater. Sci.* **2010**, *50*, 612–621. [CrossRef]
17. Jin, X.; Huo, L.; Yu, H.; Bai, B.; Li, X.; Cao, J. Numerical simulation of parameter of residual stresses on butt-welded duplex stainless steel pipes. *J. Tianjin Univ.* **2004**, *37*, 116–125.

18. Lee, C.H.; Chang, K.H. Comparative study on girth weld-induced residual stresses between austenitic and duplex stainless steel pipe welds. *Appl. Therm. Eng.* **2014**, *63*, 140–150. [CrossRef]
19. *KS D 0026 (ISO 783)*; Method of Elevated Temperature Tensile Test for Steels and Heat-Resisting Alloys. Korean Standards: Seoul, Republic of Korea, 2002.
20. Lee, C.H. Computational modelling of the residual stress evolution due to solid-state phase transformation during welding. *Model. Simul. Mater. Sci. Eng.* **2008**, *16*, 075003. [CrossRef]
21. Arun, D.; Devendranath Ramkumara, K.; Vimala, R. Multi-pass arc welding techniques of 12 mm thick super-duplex stainless steel. *J. Mater. Process. Technol.* **2019**, *271*, 126–143. [CrossRef]
22. Chandra Sekhara Rao, P.V.; Manoj, A.; Renuka Swathi, B. Residual stress measurement of Inconel 600 on different welding techniques by using conventional and XRD method. *Mater. Today Proc.* **2021**, *41*, 1160–1163. [CrossRef]
23. Sattari-Far, I.; Javadi, Y. Influence of welding sequence on welding distortions in pipes. *Int. J. Press. Vessel. Pip.* **2008**, *85*, 265–274. [CrossRef]
24. Del Coz Díaz, J.J.; Menéndez Rodríguez, P.; García Nieto, P.J.; Castro-Fresno, D. Comparative analysis of TIG welding distortions between austenitic and duplex stainless steels by FEM. *Appl. Therm. Eng.* **2010**, *30*, 2448–2459. [CrossRef]
25. Haz Metal. Stainless Steels and Their Properties. 2013. Available online: http://www.hazmetal.com/f/kutu/1236776229.pdf (accessed on 10 January 2024).
26. Barsoum, Z. Residual stress analysis and fatigue of multi-pass welded tubular structures. *Eng. Fail. Anal.* **2008**, *15*, 863–874. [CrossRef]
27. Teng, T.L.; Chang, P.H.; Tseng, W.C. Effect of welding sequence on residual stresses. *Comput. Struct.* **2003**, *81*, 273–286. [CrossRef]
28. Taljat, B.; Radhakrishnan, B.; Zacharia, T. Numerical analysis of GTA welding process with emphasis on post -solidification phase transformation effects on the residual stresses. *Mater. Sci. Eng. A* **1998**, *246*, 45–54. [CrossRef]
29. Lee, C.H. A Study on the Mechanical Characteristics of High Strength Steel for the Application to the Steel Bridge. Ph.D. Thesis, Chung-Ang University, Seoul, Republic of Korea, 2005.
30. Pardo, E.; Weckman, D.C. Prediction of weld pool and reinforcement dimensions of GMA welds using a finite element model. *Metall. Mater. Trans.* **1989**, *20B*, 937–947. [CrossRef]
31. Lindgren, L.-E. Finite element modelling and simulation of welding, Part 2 Improved material modeling. *J. Therm. Stress.* **2001**, *24*, 195–231. [CrossRef]
32. Bathe, K.J. *Finite Element Procedures*; Prentice Hall: Saddle River, NJ, USA, 1996.